ADVANCES IN ATMOSPHERIC SCIENCES, VOL. 32, DECEMBER 2015, 1669–1682

Predictability of the Summer East Asian Upper-Tropospheric Westerly Jet in ENSEMBLES Multi-Model Forecasts

LI Chaofan[1] and LIN Zhongda*[2]

[1]*Center for Monsoon System Research, Institute of Atmospheric Physics, Chinese Academy of Sciences, Beijing* 100029

[2]*State Key Laboratory of Numerical Modelling for Atmospheric Sciences and Geophysical Fluid Dynamics, Institute of Atmospheric Physics, Chinese Academy of Sciences, Beijing* 100029

(Received 16 February 2015; revised 12 May 2015; accepted 10 June 2015)

ABSTRACT

The interannual variation of the East Asian upper-tropospheric westerly jet (EAJ) significantly affects East Asian climate in summer. Identifying its performance in model prediction may provide us another viewpoint, from the perspective of upper-tropospheric circulation, to understand the predictability of summer climate anomalies in East Asia. This study presents a comprehensive assessment of year-to-year variability of the EAJ based on retrospective seasonal forecasts, initiated from 1 May, in the five state-of-the-art coupled models from ENSEMBLES during 1960–2005. It is found that the coupled models show certain capability in describing the interannual meridional displacement of the EAJ, which reflects the models' performance in the first leading empirical orthogonal function (EOF) mode. This capability is mainly shown over the region south of the EAJ axis. Additionally, the models generally capture well the main features of atmospheric circulation and SST anomalies related to the interannual meridional displacement of the EAJ. Further analysis suggests that the predicted warm SST anomalies in the concurrent summer over the tropical eastern Pacific and northern Indian Ocean are the two main sources of the potential prediction skill of the southward shift of the EAJ. In contrast, the models are powerless in describing the variation over the region north of the EAJ axis, associated with the meridional displacement, and interannual intensity change of the EAJ, the second leading EOF mode, meaning it still remains a challenge to better predict the EAJ and, subsequently, summer climate in East Asia, using current coupled models.

Key words: East Asian westerly jet, seasonal prediction, coupled model, meridional displacement

Citation: Li, C. F., and Z. D. Lin, 2015: Predictability of the summer East Asian upper-tropospheric westerly jet in ENSEMBLES multi-model forecasts. *Adv. Atmos. Sci.*, **32**(12), 1669–1682, doi: 10.1007/s00376-015-5057-z.

1. Introduction

The East Asian upper-tropospheric westerly jet (EAJ), one of the most important components in the Asian monsoon system, is intimately related to the East Asian climate anomalies in boreal summer (Lin, 2013; Lu et al., 2013). The interannual variations in both the EAJ location and intensity correspond closely to the rainfall and surface air temperature anomalies over East Asia, especially for the meridional displacement of the EAJ location (Lau et al., 2000; Lu, 2004; Wang et al., 2013). The poleward displacement of the EAJ tends to be linked to deficient rainfall along the East Asian subtropical rainy belt (Lau et al., 2000) and more frequent high temperature extremes in Southeast China (Wang et al., 2013). Thus, interannual variation of the EAJ is expected to have some implications for the predictability of summer climate anomalies over East Asia (Liang and Wang, 1998; Zhang and Guo, 2005). As the current status of seasonal prediction for East Asian summer rainfall remains a challenge, it is imperative to comprehensively assess the prediction of the summer EAJ.

The interannual variation of the EAJ is characterized by meridional displacement of the EAJ location and intensity change, which are the first and second leading EOF modes of the EAJ, respectively (Lin and Lu, 2005). The atmospheric circulation anomalies related to the meridional shift of the EAJ location involve two wave trains: the Pacific–Japan (PJ) teleconnection (Nitta, 1987; Kosaka and Nakamura, 2006; Lu and Lin, 2009) or the East Asia–Pacific (EAP) teleconnection (Huang and Sun, 1992; Huang, 2004) in the meridional direction over the East Asia–western North Pacific (WNP) region, and the "Silk Road" teleconnection in the zonal direction along the upper-tropospheric Asian westerly jet (Lu et al., 2002; Enomoto et al., 2003; Enomoto, 2004; Ding and Wang, 2005). In addition, the transient eddy forcing also demonstrates significant impact on the meridional displacement of the EAJ, especially its northward progression (Xiang and Yang, 2012). On the other hand, Lu (2004) also revealed a significant meridional connection of the EAJ in-

* Corresponding author: LIN Zhongda
Email: zdlin@mail.iap.ac.cn

tensity change with convective activities over the Philippine Sea, though it is weaker than that related to the meridional displacement of the EAJ location.

Despite all the above atmospheric forcing, the interannual meridional displacement of the EAJ location is also influenced by the tropical SST anomalies. Lin (2010) found that, associated with the southward shift of the EAJ in July and August, a warm SST anomaly in the tropical eastern Pacific persists from the preceding spring to the concurrent summer. Additionally, Qu and Huang (2012) revealed that the SST anomalies over the tropical Indian Ocean are also significantly related to the meridional displacement of the EAJ. When SST warms in the tropical Indian Ocean, especially the northern Indian Ocean (NIO), the EAJ shifts southward.

However, atmospheric general circulation models (AGCMs) are deficient in describing the SST-induced interannual variation of the EAJ. Lu et al. (2006) investigated the external and internal atmospheric variability over the WNP and East Asia based on the simulations forced by the prescribed observed SST in the Met Office AGCM, known as HadAM3. They indicated that the interannual anomalies of the EAJ, including both meridional displacement of the EAJ location and its intensity change, are dominated by atmospheric internal variability, different from the lower-tropospheric circulation anomaly over the WNP, in which external variability plays an important role. The strong effect of the internal variability suggests a low potential predictability of the EAJ variation in the AGCM. In addition, current AGCMs are unable to properly simulate the Asian summer monsoon rainfall because the ocean–atmosphere coupling contributes significantly to the climate anomalies over the WNP and East Asia (Wang et al., 2004, 2005). This will further increase the possibility of AGCM deficiencies in the prediction of the summer EAJ, in terms of the meridional teleconnection between the interannual variation of the EAJ and convective activities over the WNP and East Asia. As a consequence, ocean–atmosphere coupled general circulation models (CGCMs) are more appropriate for the prediction of the interannual variation of the summer EAJ.

Some studies have analyzed the potential predictability of summer climate and circulation anomalies in the Northern Hemisphere in CGCMs (Chowdary et al., 2010; Lee et al., 2011; Kosaka et al., 2012; Li et al., 2012, 2014). Their results imply that atmosphere–ocean interactions, induced by the tropical Indian and Pacific oceans, contribute remarkably to the prediction reliability. Lee et al. (2011), for example, examined the predictability of summer upper-tropospheric circulation in the Northern Hemisphere. They pointed out that the seasonal forecast skill for the 200 hPa geopotential height derived mainly from the CGCM's ability to predict the first two EOF modes in the Northern Hemisphere, for the 25-year period of 1981–2005. The first two EOF modes are characteristics of zonally uniform anomalies of upper-tropospheric geopotential height over the tropics (EOF1), due to the prolonged impact of El Niño–Southern Oscillation (ENSO), and over the midlatitudes (EOF2) related to the developing ENSO. The zonally uniform anomalies of geopotential height at 200 hPa suggest a potential predictability of upper-tropospheric zonal winds in the context of geostrophic wind balance. Nevertheless, the current status of the seasonal predictability of the EAJ variation by CGCMs remains unclear and has not yet been well documented in the literature.

Recently, the ENSEMBLES project (ensembles-based predictions of climate changes and their impacts), advocated by the European Union (van der Linden and Mitchell, 2009), provided seasonal multi-model prediction products of five leading CGCMs developed in Europe for the period 1960–2005. Based on the retrospective forecast (hindcast) of ENSEMBLES, Li et al. (2012) investigated the prediction of the summer WNP subtropical high and suggested that ENSEMBLES shows considerable capability in describing the interannual variation of the summer lower-tropospheric circulation and precipitation anomalies over the WNP. Moreover, related to the WNP subtropical high, the meridional teleconnection, in the lower troposphere, can be captured by these coupled models.

This study attempts to comprehensively assess the predictability of the interannual variation of the EAJ, based on the products of the ENSEMBLES forecast system. Assessment of the EAJ will hopefully provide us another viewpoint, from the perspective of upper-tropospheric circulation, on the seasonal predictability of the summer monsoon and rainfall over East Asia. The rest of this paper is organized as follows. Section 2 describes the model hindcasts and observed datasets used in this study. Section 3 presents the comprehensive assessment of the EAJ, including its climatology, interannual variability, temporal correlation coefficients, two leading EOF modes, circulation and tropical SST anomalies associated with the meridional displacement of the EAJ location. The predicted decadal change and potential prediction skill of the EAJ location and its implications are discussed in section 4. Conclusions are summarized in section 5.

2. Model hindcasts and observational datasets

The ENSEMBLES project was a seasonal-to-annual multi-model project developed by the European Union (van der Linden and Mitchell, 2009). It comprised five fully coupled atmosphere–ocean models, including the UK Met Office (UKMO), the Météo-France (MF), the European Centre for Medium-Range Weather Forecasts (ECMWF), the Leibniz Institute of Marine Sciences at Kiel University (IFM-GEOMAR) and the Euro-Mediterranean Center for Climate Change (CMCC-INGV). The atmosphere and ocean were initialized using realistic estimates of their observed states. All of these models included major radiative forcing and had no flux adjustments. An ensemble of nine initial conditions was run for each model. Further details on the ENSEMBLES multi-model project, the models and the initial condition perturbations can be found in Weisheimer et al. (2009) and Doblas-Reyes et al. (2010).

A 46-year hindcast from 1960 to 2005 was carried out in the five models. They were initialized on 1 May for each

year and run for seven months. The hindcast results for June, July and August are analyzed in this study. Additionally, the multi-model-ensemble (MME) results are calculated through a simple composite by applying equal weight to all the five models.

The observational datasets used here for validating the model simulation include: (1) National Centers for Environmental Prediction/National Center for Atmospheric Research (NCEP/NCAR) monthly reanalysis data from 1960 to 2005 (Kalnay et al., 1996); (2) National Oceanic and Atmospheric Administration Extended Reconstructed monthly mean SST V3 data from 1960 to 2005 (Smith and Reynolds, 2004); and (3) monthly precipitation data obtained from the Global Precipitation Climatology Project during 1979–2005 (Adler et al., 2003).

3. Results

In this section, we show the performance of the prediction of the EAJ in the five models in ENSEMBLES. The predicted climatology and interannual standard deviation are presented in subsection 3.1, the prediction skill of the interannual variation of the EAJ in subsection 3.2, and the circulation and SST anomalies associated with the meridional shift of the EAJ location in subsections 3.3 and 3.4.

3.1. *Climatology and interannual variability*

Figure 1 shows the climatology of JJA (June–July–August)-mean 200 hPa zonal wind. In the observation, the upper-tropospheric jet stream is basically zonally oriented over East Asia. The axis of the EAJ, with the maximum 200 hPa zonal wind in each longitude over East Asia, is located at approximately 40°N (Fig. 1a). The above features of the EAJ are successfully captured by the five models and the MME prediction (Figs. 1b–g). The location and intensity of the summer-mean EAJ described by the models are closely consistent with those shown in the observation, with a pattern correlation coefficient ranging from 0.96 to 0.98. The MME prediction performs generally better than the individual models, as it can reduce the noise presented in the individual forecasts. Relatively, the intensity of the JJA-mean zonal wind over East Asia is a little stronger in the ECMWF and IFM-GEOMAR models and weaker in the CMCC-INGV model. The axis of the EAJ is located a little south in the MF model than that in the observation.

The interannual variation of upper-tropospheric zonal wind, during 1960–2005 in the observation, mostly appears in the midlatitudes between 20°N and 60°N, with two maxima residing to the south and north sides of the EAJ axis, respectively (Fig. 2a). The maximum interannual standard deviation is greater than 3.5 m s^{-1} both to the north and south sides of the EAJ axis. In terms of the model predictions, though it is weaker than observed, the maximum standard deviation, greater than 2 m s^{-1} in the five models and 1.5 m s^{-1} in their MME prediction, is captured over the region south of the EAJ axis (Figs. 2b–g). The result suggests these current coupled models show certain capability in capturing the interannual variation of the EAJ, particularly when it shifts southward. On the other hand, the standard deviation to the north of the EAJ axis is much weaker than that in the observation. This weaker variability is related to the ensemble mean of different initial conditions for the model prediction, and it further suggests that many synoptic perturbations contribute to the variations of the EAJ, especially to the north of the EAJ axis (e.g., Dole and Black, 1990; Wu et al., 2006; Xiang and Yang, 2012). This is also the reason that the interannual variability of the MME prediction is a little weaker than that of the five individual models. Among the five models, the MF model (Fig. 2e) predicts a weaker standard deviation over East Asia than the other four models.

3.2. *Prediction skill of the EAJ interannual variation*

Figure 3 illustrates the spatial distribution of the temporal correlation coefficient (TCC) between the model predictions and observation for 200 hPa zonal wind during 1960–2005. The MME prediction performs generally the best (Fig. 3a). Good predictions of the upper-tropospheric zonal wind are found mainly over the south of the EAJ axis, extending northeastward from India to Japan, where the TCC skill over most of these regions is significant at the 95% confidence level in the MME and all five models except for the MF model. Consistent with the performance of the interannual variability (Fig. 2e), the MF model exhibits relatively weaker capability in describing the variation of 200 hPa zonal wind over East Asia and the good prediction skill is unable to extend northeastward to North China and Japan (Fig. 3d). Compared with that south of the EAJ axis, the skill over the region north of the EAJ axis is lower, though certain skill is also found over the north of the EAJ axis, especially over the east of Lake Baikal, in the MME, ECMWF, IFM-GEOMAR, and UKMO predictions. It is interesting to note that good predictions are located on the two sides of the EAJ axis, not in the axis region itself. This may suggest that the coupled models tend to better predict the meridional displacement of the EAJ location rather than its intensity change.

Next, we investigate how well the models hindcasts describe the dominant modes of the year-to-year variability of the summer 200 hPa zonal wind over East Asia. To identify the major modes of the EAJ, we apply EOF analysis to the JJA 200 hPa zonal wind over the region (27.5°–55°N, 120°–150°E), with strong interannual variability (Fig. 2), following Lin and Lu (2005).

Figure 4 shows the spatial distribution of the first leading EOF mode (EOF1) of the JJA 200 hPa zonal wind for the observation, the MME and the predictions of the five models. EOF1, which accounts for 50% of the total variance in the observation, is characterized by the meridional variation of the EAJ location, with positive (negative) anomalies to the south (north) of the EAJ axis (Fig. 4a). The models show good capability in describing the spatial distribution of EOF1 (Figs. 4b–g). Variation of the EAJ meridional displacement for the model prediction averaged by different ensemble members accounts for a much larger variance, especially for the MME

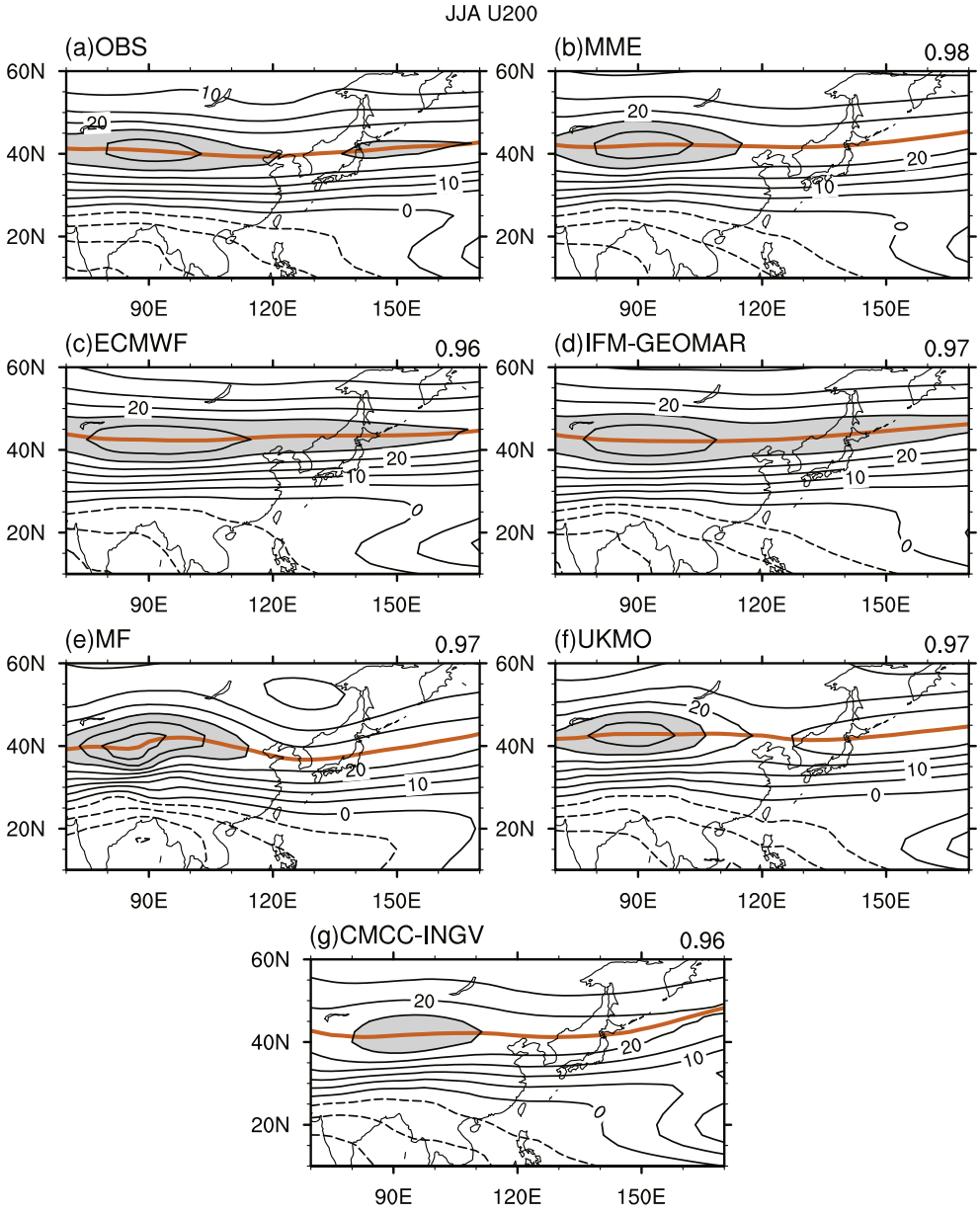

Fig. 1. Climatology of the JJA-mean 200 hPa zonal wind (units: m s^{-1}) for (a) the observation, and the prediction of (b) the MME and (c–g) the five models of ENSEMBLES during 1960–2005. The value in the upper-right corner is the pattern correlation coefficient between the observation and model prediction. Shading indicates the region where the value exceeds 20 m s^{-1} and the orange solid line represents the location of the EAJ axis.

prediction that comprises more members. This suggests that these coupled models are apt at reproducing the distribution pattern for this variation. Nevertheless, the models slightly overestimate the variation of the positive anomalies over the southern extent and underestimate the negative anomalies over the northern extent. This corresponds well to the interannual variability exhibited by the models, as stronger variability is found to the south than the north side of the EAJ axis (Figs. 2b–g).

The models are also capable of predicting the temporal evolution corresponding to EOF1 (Table 1). The correlation coefficient of the associated principal component time series (PC1) between the MME prediction and the observation is 0.4, which is significant at the 99.5% confidence level. Similarly, most of the five models, except for the MF model, show similarly good capabilities. The IFM-GEOMAR model performs the best among the five models and the prediction correlation coefficient reaches 0.5. The prediction correlation coefficient of 0.28 for the ECMWF and UKMO models exceeds the 94% confidence level, but is not greater than the 95% confidence level. The good performance of the coupled models in terms of EOF1 offers certain realizable predictability of the interannual meridional variation of the EAJ location.

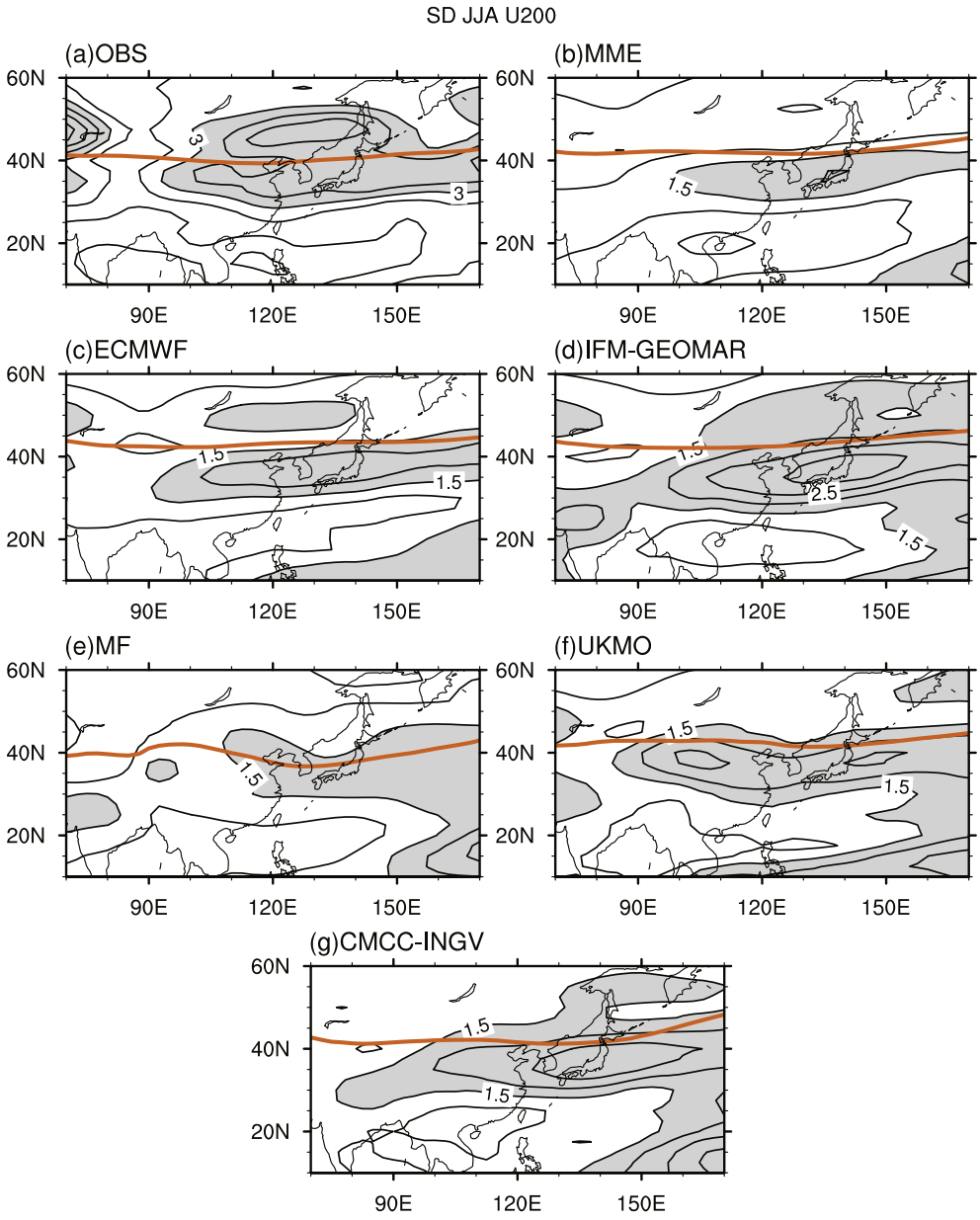

Fig. 2. As in Fig. 1, but for interannual standard deviation of the JJA-mean 200 hPa zonal wind. Shading indicates regions with values greater than 3 m s^{-1} for the observation in (a) and 1.5 m s^{-1} for the model predictions in (b–g).

Table 1. Correlation coefficients of the first two principal components (PC1 and PC2) between the observation and model predictions. The values in bold and those underlined represent statistical significance exceeding the 99% and 95% confidence levels, respectively.

Corr.	MME	ECMWF	IFM-GEOMAR	MF	UKMO	CMCC-INGV
PC1	**0.40**	0.28	**0.50**	0.14	0.28	<u>0.32</u>
PC2	0.00	0.08	0.07	−0.08	−0.07	0.11

The second dominant mode (EOF2) features the changes of the EAJ intensity (Fig. 5). It is associated with significant positive values along the EAJ axis, accounting for 21.8% of the total variance in the observation. In general, a few models, including the ECMWF and IFM-GEOAR models, and the MME, tend to properly reproduce the spatial distribution of the EOF2 mode, but with a smaller explainable variance (Figs. 5b–d). The other three models show similar explainable variance to the observation, but the positive anomalies extend more northward than the observation (Figs. 5e–g), which contribute significantly to the northward distribution of the positive anomalies in the MME prediction (Fig. 5b). In addition, the models are powerless in describing the interannual variation of the associated PC time series for the EOF2 mode (PC2). The correlation coefficients are around zero for

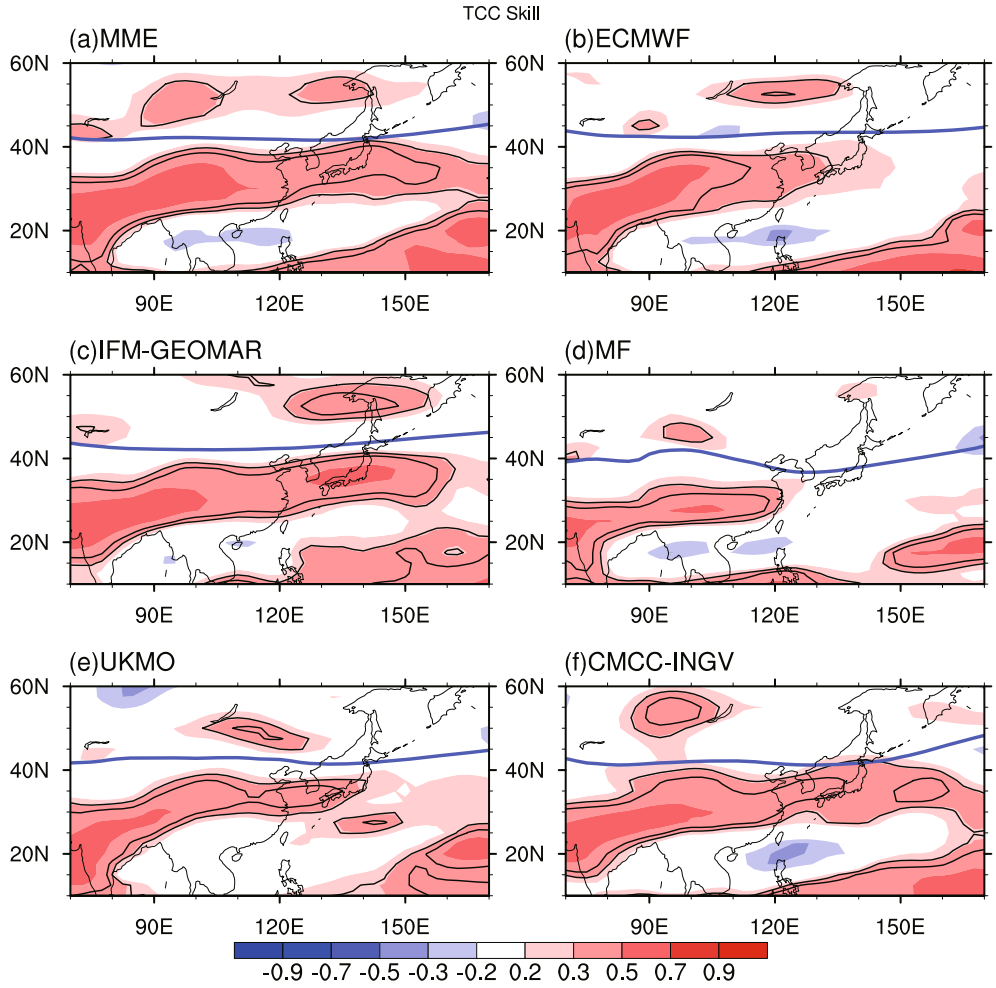

Fig. 3. Temporal correlation coefficients of the JJA-mean 200 hPa zonal wind between the observation and prediction of (a) the MME, and (b–f) the five models. Contours represent statistical significance of the correlation coefficients at the 95% and 99% confidence levels and the thick blue line represents the location of the EAJ axis.

the predictions of the MME and five models (Table 1). Thus, the current coupled models have difficulty in capturing the interannual intensity change of the EAJ.

3.3. *Circulation anomalies related to the meridional shift of the EAJ location*

Lu (2004) defined an index to depict the meridional shift of the EAJ location by the difference of 200 hPa zonal winds averaged over 120°–150°E between 10° to the south of the EAJ axis and 10° to the north. Similarly, we define a JJA-mean EAJ location index (EAJLI) as the difference of 200 hPa zonal winds averaged between the regions (30°–40°N, 120°–150°E) and (40°–50°N, 120°–150°E). Indeed, this EAJLI depicts the first EOF leading mode of interannual variations of the EAJ (Lin and Lu, 2005). The EAJ moves southward when the EAJLI is positive, and it shifts northward when the EAJLI is negative. Time series of the EAJLI in the observation, MME, and five models are shown in Fig. 6. The correlation coefficient between the EAJLI and PC1 is 0.92 in the observation, 0.96 in the MME, and larger than 0.9 in all of the five models for the period 1960–2005. In the following analysis, the EAJLI, instead of PC1, is used to depict meridional shift of the EAJ location because it is more convenient to discuss the relative contribution from 200 hPa zonal winds on the southern (30°–40°N, 120°–150°E) and northern (40°–50°N, 120°–150°E) sides, respectively.

The prediction skill of the EAJLI is presented in Table 2. The correlation coefficient of the EAJLI between the MME and observation is 0.35 during 1960–2005, which is significant at the 95% confidence level. Similarly, significant correlation coefficients are also found in the IFM-GEOMAR

Table 2. Correlation coefficients of the EAJ location index (EAJLI) and its two sides between the observation and model predictions. The values in bold and those underlined represent statistical significance exceeding the 99% and 95% confidence levels, respectively.

Corr.	MME	ECMWF	IFM-GEOMAR	MF	UKMO	CMCC-INGV
EAJLI	<u>0.35</u>	0.19	<u>0.31</u>	0.07	<u>0.34</u>	0.27
Southern	**0.51**	<u>0.33</u>	**0.59**	0.22	**0.38**	**0.44**
Northern	0.06	0.01	−0.01	−0.10	0.17	0.09

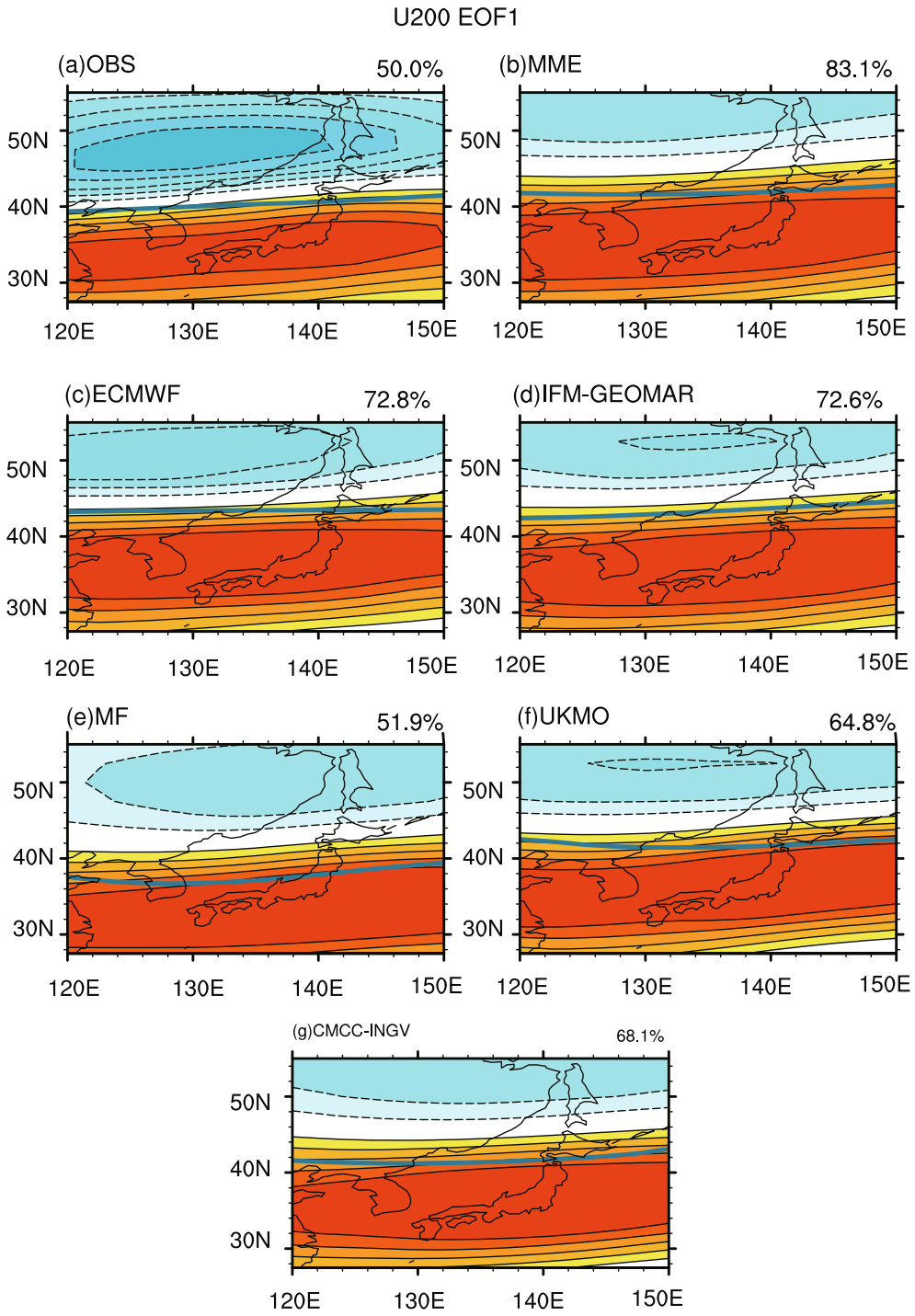

Fig. 4. Spatial distribution of the first EOF mode of the JJA-mean 200 hPa zonal wind over East Asia for (a) the observation, (b) the MME and (c–g) the five model predictions. The percentage value in the upper-right corner shows the percentage variance explained by this mode and the thick blue line represents the location of the EAJ axis.

(0.31) and UKMO (0.34) models, at the 95% confidence level, and in the CMCC-INGV (0.27) model, at the 90% confidence level. The skill of the EAJLI is mainly attributed to that of the southern side. The correlation coefficient of the southern side is 0.51 in the MME, 0.59 in the IFM-GEOMAR model, 0.38 in the UKMO model, and 0.44 in the CMCC-INGV model, all significant at the 99% confidence level. For the other two models, the correlation coefficient of the southern side is 0.33 in the ECMWF model, significant at the 95% confidence level, and 0.22 in the MF model, though the correlation coefficients of the corresponding EAJLI for these two models are only 0.19 and 0.07, respectively. However, the prediction skill of the northern side is poor, with a maximum correlation coefficient of 0.17 and minimum of −0.1

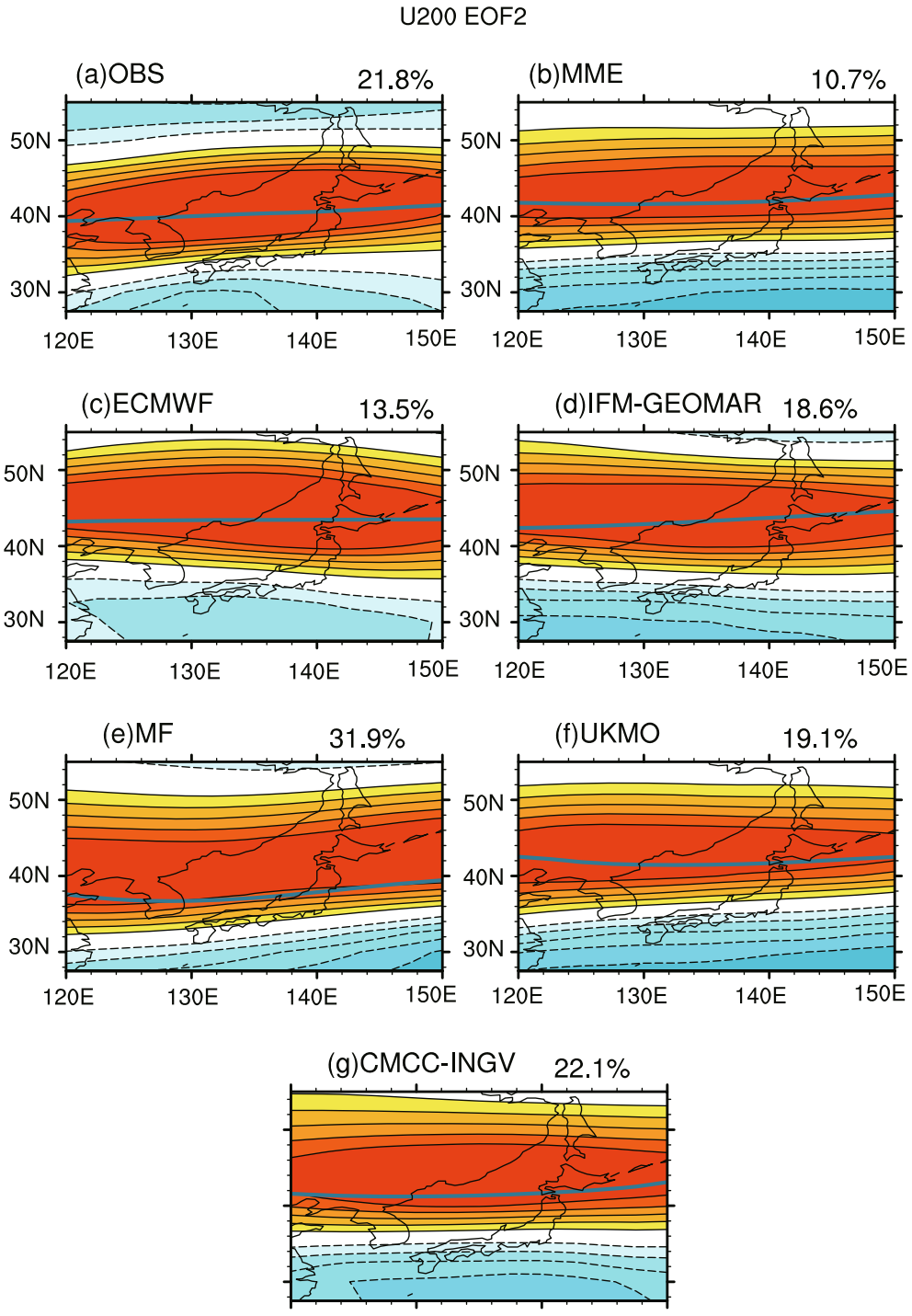

Fig. 5. As in Fig. 4, but for the second EOF mode.

between the observation and the five individual models and their MME.

Further analysis shows that the main features of the circulation anomalies in the upper and lower troposphere, related to the EAJLI, are well predicted by the models, as illustrated in Fig. 7. In the observation, associated with the EAJLI are a westerly anomaly to the south of 40°N and an easterly anomaly to the north over East Asia in the upper troposphere (Fig. 7a), consistent with a southward shift tendency of the EAJ. In addition, the westerly and easterly wind anomalies over East Asia extend westward into West Asia so that the Asian westerly jet together moves southward. In the lower troposphere, a meridional wave train is observed, with a cyclonic anomaly over East Asia and an anticyclonic anomaly over the western North Pacific (WNP), i.e., the PJ or EAP pattern. This meridional connection between the EAJ and the lower-tropospheric circulation anomalies over the East Asia–WNP region is consistent with the result previously identified

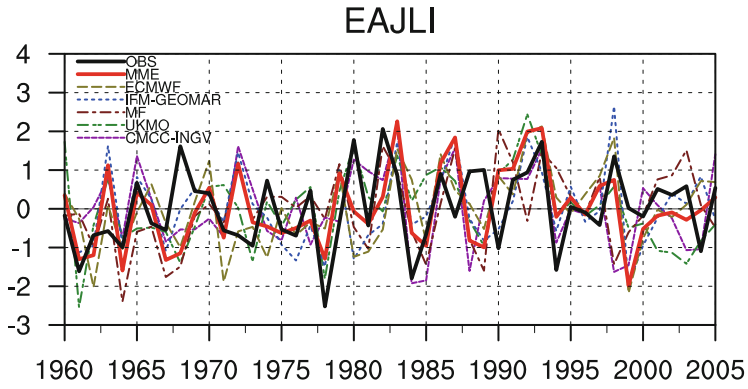

Fig. 6. Normalized time series of the EAJLI during 1960–2005 for the observation and model predictions.

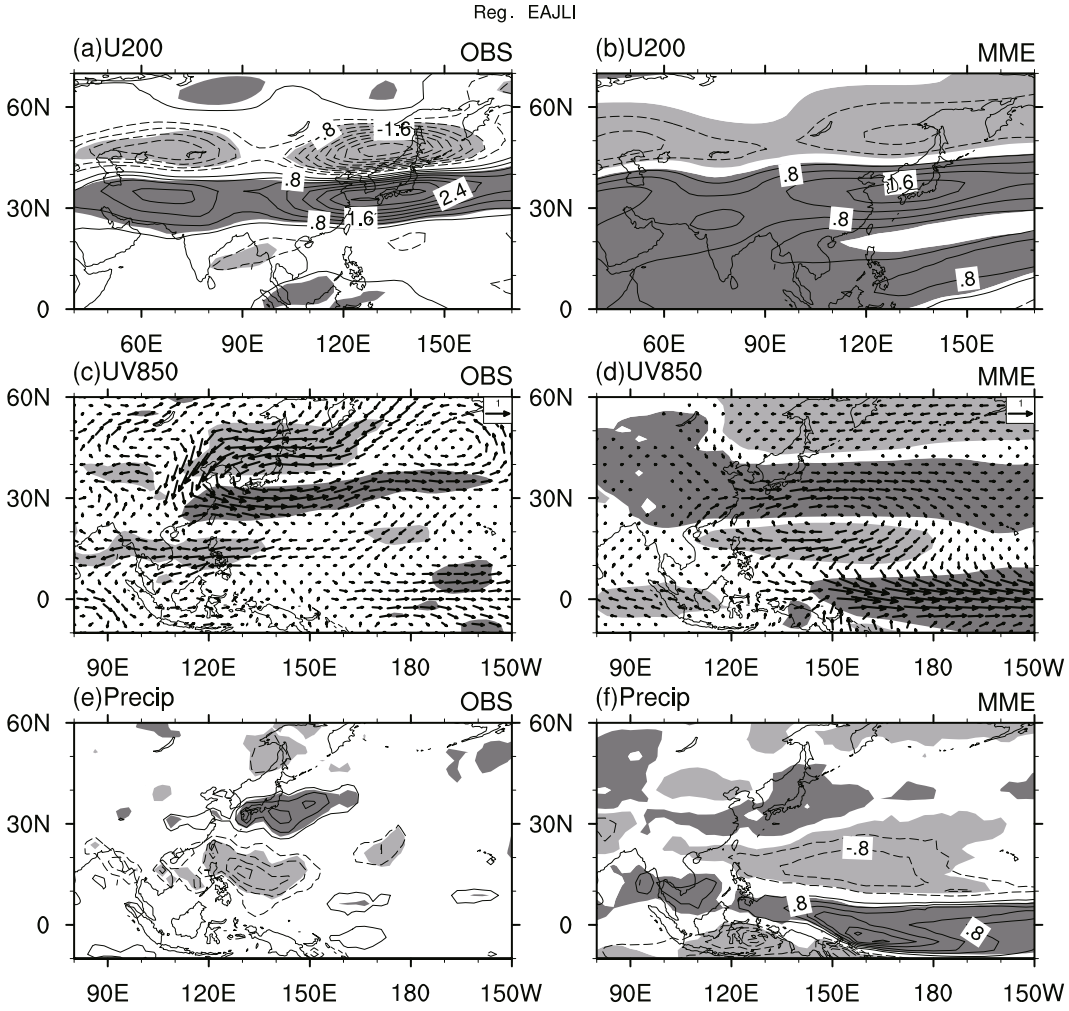

Fig. 7. Regression of the (a, b) 200 hPa zonal wind, (c, d) 850 hPa wind and (e, f) precipitation anomalies onto the normalized EAJLI in the (a, c, e) observation and (b, d, f) MME prediction. Shading indicates the region where the anomaly exceeds the 95% confidence level. The contour interval of the 200 hPa zonal wind (precipitation) anomaly is 0.4 m s^{-1} (0.4 mm d^{-1}).

by Lu and Lin (2009). Associated with the meridional connection, rainfall is enhanced over East Asia and suppressed over the WNP, Northeast China, and southern Russia (Fig. 7e).

The circulation anomalies in the upper and lower troposphere and rainfall anomalies related to the EAJLI, discussed above in the observation, are successfully captured by the model predictions. In the MME prediction, associated with

the EAJLI, the Asian westerly jet moves southward in the upper troposphere (Fig. 7b) and the meridional connection is established with a cyclonic anomaly over East Asia and an anticyclonic anomaly over the WNP in the lower troposphere (Fig. 7d). Meanwhile, rainfall increases over East Asia and decreases over the WNP (Fig. 7f). The successful reproducibility of the enhanced rainfall over East Asia further presents an implication for the important contribution of the EAJ displacement to the East Asian summer prediction. However, the relationship between the EAJ and tropical anomalies from the East Indian Ocean to the western Pacific, in the MME prediction, is significantly strengthened, compared with that in the observation. Related to the EAJLI, in the MME prediction, there are significant westerly anomalies over the tropical regions in the upper troposphere (Fig. 7b), and westerly anomalies over the tropical western Pacific and easterly anomalies over the East Indian Ocean in the lower troposphere (Fig. 7d), concurrent with increased rainfall in the tropical western Pacific and decreased rainfall over the Maritime Continent (Fig. 7f). This enhanced EAJLI–tropics connection is due to the overestimated effect of the tropical SST in the central-eastern Pacific and Indian Ocean in the model predictions, which is discussed in the next subsection.

3.4. *Tropical SST-EAJ location relationship*

The next step is to investigate what is responsible for the prediction skill of the EAJLI. To explore the possible impact of external forcing, we regress JJA-mean SST anomalies onto the EAJLI in the observation (Fig. 8a) and the MME prediction (Fig. 8b). As shown in Fig. 8a, in the observation, the southward shift of the EAJ is significantly correlated with simultaneous warm SST anomalies in the tropical eastern Pacific and Indian Ocean, especial the northern Indian Ocean (NIO).

The tropical SST anomalies depicted above are successfully reproduced in the MME prediction (Fig. 8b), including the warm SST anomalies in the tropical eastern Pacific and NIO. This result therefore suggests a possible role of the tropical SST anomalies in the prediction of the EAJ location. However, the signals are much stronger in the model predictions than in the observation, arising from the average of different ensemble members in the model predictions. Here, we use two SST indices, the Niño3 index and NIO index (NIOI), to represent the interannual variation of SST in the tropical eastern Pacific and NIO, respectively. The Niño3 index is defined as the JJA-mean SST anomalies averaged over the region (5°S–5°N, 90°–150°W) and the NIOI over the region (0°–20°N, 40°–100°E). The correlation coefficient between the EAJLI and Niño3 index increases from 0.26 in the observation to 0.73 in the MME, and it ranges from 0.35 to 0.66 in the five individual models (Table 3). Similarly, the correlation coefficient between the EAJLI and NIOI rises from 0.44 in the observation to 0.67 in the MME, and it changes from 0.52 to 0.63 in all of the models except the UKMO (0.44) and CMCC-INGV (0.39) models (Table 3).

To confirm the crucial role of the tropical SST anomalies of the eastern Pacific and NIO in the prediction of the EAJ location, we build a multiple linear regression model based on the predicted JJA Niño3 index and NIOI, to statistically predict the EAJLI. Accordingly, the statistical prediction skill of the EAJLI is due to the linear contribution of the dynamically predicted tropical eastern Pacific and NIO SST anomalies in

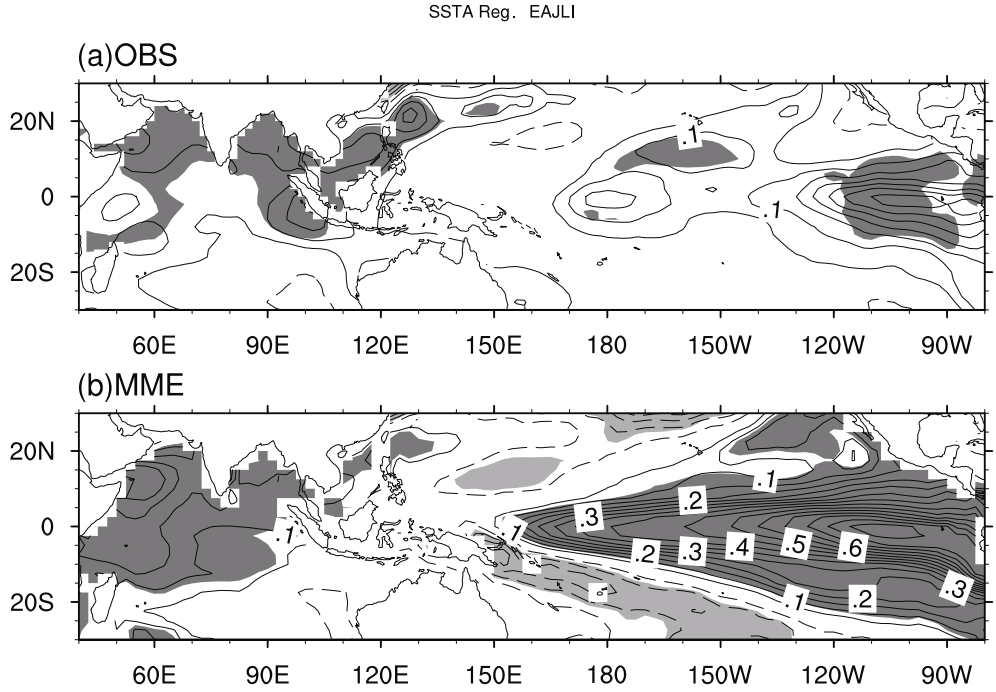

Fig. 8. Regression of the SST anomalies onto the normalized EAJLI in the (a) observation and (b) MME prediction. Shading indicates the regions where the anomaly exceeds the 95% confidence level, and the contour interval is 0.05°C.

Table 3. Correlation coefficients between the EAJLI and SST anomalies averaged over the Niño3 and NIO region.

Corr.	Niño 3	northern Indian Ocean
OBS	0.26	0.44
MME	0.73	0.67
ECMWF	0.35	0.61
IFM-GEOMAR	0.63	0.63
MF	0.47	0.52
UKMO	0.43	0.44
CMCC-INGV	0.66	0.39

the MME prediction. The cross-validated time series of the statistically predicted EAJLI are presented in Fig. 9. Its correlation coefficient with the observation is 0.32, close to the value of 0.35 between the MME prediction and the observation during 1960–2005. Moreover, the cross-validated EAJLI agrees well with the MME-predicted EAJLI, with a correlation coefficient of 0.72 between them, indicating that about half of the predicted variance of the EAJLI is contributed linearly by the predicted tropical SST anomalies in the eastern Pacific and NIO in the MME.

The SST anomalies associated with the summertime EAJLI were also revealed by Lin (2010), particularly in July and August. Lin (2010) proposed that the tropical eastern Pacific warm SST anomaly links to a southward shift of the EAJ through a meridional teleconnection over the WNP–East Asia region, which is associated with increased precipitation over the tropical western Pacific and decreased precipitation over the subtropical WNP. The rainfall anomalies are partially indicated by the EAJLI-related rainfall in the MME prediction, as shown in Fig. 7f. On the other hand, Shaman and Tziperman (2007) additionally highlighted the role of the westward propagating Rossby wave, induced by the tropical eastern Pacific warm SST-related divergence forcing over the equatorial Pacific in the upper troposphere. This interacts with the North Africa–Asia westerly jet and manifests as positive vorticity anomalies along the westerly jet, causing the southward shift of the EAJ.

Furthermore, Qu and Huang (2012) also found a positive correlation between the warm NIO SST anomalies and southward shift of the EAJ. They proposed that when the tropical Indian Ocean SST is higher than normal, the anomalous tropical convection forces a Kelvin wave wedge penetrating into the equatorial western Pacific, leading to a decrease in precipitation near the Philippines (Xie et al., 2009). Combined with the climatological easterly shear over the subtropical WNP (Lim and Chang, 1983, 1986; Wang and Xie, 1996; Lu, 2004; Lin, 2010), the EAP teleconnection (Huang and Sun, 1992) is induced along the East Asian coast, which accelerates westerly on the southern flank of the EAJ and decelerates westerly on the northern flank in the upper troposphere (Kosaka and Nakamura, 2006; Lu and Lin, 2009). Thus, the EAJ shifts southward.

Furthermore, the anomalous SSTs show a much stronger teleconnection with the 200 hPa zonal winds on the southern side of the EAJ axis than on its northern side. The correlation coefficient between the southern side of the EAJ axis and the Niño3 (NIO) SST anomalies is 0.50 (0.47) in the observation. This close teleconnection is reproduced by the model; the corresponding correlation coefficients are both 0.73 in the MME prediction, presenting more predictable signals of the wind anomalies over the region. However, the correlation coefficient between the northern side of the EAJ axis and the Niño3 (NIO) SST anomalies is only 0.07 (−0.20) in the observation and 0.37 (0.25) in the MME prediction. The stronger relationship to the southern side of the EAJ axis of zonal winds at 200 hPa with the tropical SST anomalies, leads to higher prediction skill of the southern side compared to the northern side (Table 2). The lower prediction skill on the northern side is probably due to the effect of synoptic transient activities (Xiang and Yang, 2012), which have less predictability.

4. Discussion

4.1. *Predicted decadal change of the EAJ location*

Some previous studies have reported a decadal tendency of the southward shift of the EAJ after the late 1970s (Yu and

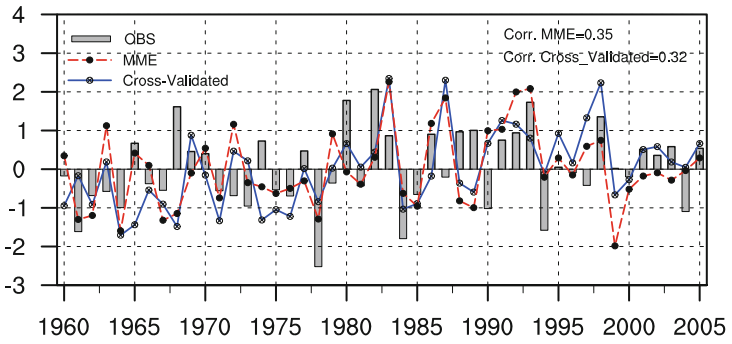

Fig. 9. Normalized time series of the EAJLI for the observation (bars), the MME prediction (red dashed line) and the statistically deduced (cross-validated, blue solid line) by the predicted Niño3 and NIO SST anomalies. The correlation coefficient between the MME predicted (cross-validated) EAJLI and the observation is 0.35 (0.32).

Zhou, 2007; Zhang and Huang, 2011). This decadal shift in the EAJ is also revealed in the observation and MME prediction of the present study (Fig. 6), suggesting a possible predicted decadal change of the EAJ location in ENSEMBLES. To reveal the predictability of decadal change of the EAJ location, we isolate the decadal component of the EAJLI, with its period longer than 8 years, based on a Fourier harmonics filter, and the residual is referred to as the interannual component.

Table 4 shows the correlation coefficients of the decadal and interannual components of the EAJLI, separately, between the observation and model simulations. The correlation coefficient of the EAJLI between the observation and MME, for the decadal component, is 0.47. Similarly, the decadal component is also predicted in the five model predictions, with the correlation coefficients ranging from 0.26 to 0.40. The potential skill of the decadal variation of the EAJLI is attributed significantly to summer SST anomalies in the tropical central-eastern Pacific and Indian Ocean, with warm tropical SST anomalies related to the southward shift of the EAJ, similar to that shown in Fig. 8. Moreover, these tropical SST anomalies can be traced back to an El Niño–like SST pattern in the previous winter (figure not shown). The positive SST anomalies may induce atmospheric warming in the tropics (Yulaeva and Wallace, 1994; Kumar and Hoerling, 2003; Huang and Huang, 2009), which increases the meridional temperature gradient in the subtropics to the south of the EAJ axis and results in a southward shift of the EAJ.

On the other hand, the potential prediction skill for the interannual component remains stable, compared with the total EAJLI. The correlation coefficient of the interannual component of the EAJLI between the MME prediction and the observation, as shown in Table 4, is 0.32, close to the value of 0.35 for the total EAJLI (Table 2), significant at the 95% confidence level. For the five models, the prediction skill of the interannual component, compared with the total EAJLI, is also stable, with a correlation coefficient with the observation of 0.35 (0.34) in the UKMO model, 0.30 (0.31) in the IFM-GEOMAR model, 0.27 (0.27) in the CMCC-INGV model, 0.13 (0.19) in the ECMWF model, and 0.0 (0.07) in the MF model, for the interannual component (total) of the EAJLI. We also regress circulation and SST anomalies upon the interannual component of the EAJLI, and obtain similar results to those in Figs. 7 and 8, except for weakened warm summer SST anomalies in the tropical eastern Pacific in the observation, suggesting a close relationship of the tropical SST anomalies in the eastern Pacific and the EAJ location on decadal timescales, as described in the above paragraph.

Table 4. Correlation coefficients of the decadal and interannual component of the EAJLI between the observation and model predictions.

Corr.	MME	ECMWF	IFM-GEOMAR	MF	UKMO	CMCC-INGV
Decadal	0.47	0.39	0.40	0.30	0.34	0.26
Interannual	0.32	0.13	0.30	0.00	0.35	0.27

4.2. *Potential prediction skill of the EAJ location*

The interannual variability of midlatitude anomalies is, generally, considered unpredictable (Lu et al., 2006; Wang, 2008; Kosaka et al., 2012). Lu et al. (2006), for example, found that the anomaly of the EAJ—both the meridional shift of the EAJ location and its intensity change—is dominated by atmospheric internal variability, different from the lower-tropospheric circulation anomaly over the WNP in which the external variability plays an important role.

In the present study, we find a correlation coefficient of 0.35 of the EAJLI during 1960–2005 between the observation and MME prediction in the previous section. It is significant at the 95% confidence level and better improved compared to that in an AGCM simulation (Lu et al., 2006). However, the potential prediction skill of the EAJLI is still lower than the WNP anomalies, with a correlation coefficient of 0.68 for the WNP summer monsoon index (Li et al., 2012) between the MME predictions and the observation. Moreover, the meridional shift of the EAJ location is successfully captured as the EOF1 mode in the five models and their MME in ENSEMBLES, the same as in the observation, while it is represented by the EOF2 mode in the SST-forced AGCM simulation in HadAM3 (Lu et al., 2006). The improved potential skill of the EAJ prediction may help increase the prediction skill of climate anomalies in East Asia, since they are closely tied on the interannual timescale (Liang and Wang, 1998; Lau et al., 2000; Lu, 2004).

5. Summary

This study investigates the predictability of the EAJ in summer based on 46-yr predictions initiated on 1 May in the five models of ENSEMBLES during 1960–2005 and NCEP/NCAR reanalysis data (taken as the observation). The results show that the five models can capture the climatological location and intensity of the summer-mean EAJ. In addition, the models also predict strong interannual standard deviation of upper-tropospheric zonal winds over East Asia to the south of the EAJ axis, though its magnitude is weaker than in the observation.

Moreover, the prediction skill for the first two EOF leading modes, i.e., the meridional displacement of the EAJ location and intensity change of the EAJ, respectively, is evaluated. The spatial pattern of the EOF1 mode is successfully captured by the five models and their MME. The temporal correlation coefficient between the observation and MME is 0.4 for the PC1 and 0.35 for the EAJ location index (EAJLI). Further examination on the two sides of the EAJLI shows that the prediction skill of the EAJLI can be attributed to that in the southern side. For the EOF2 mode, only the ECMWF and IFM-GEOMAR models, among the five, reproduce the spatial pattern of interannual intensity change of the EAJ, but none of them, including their MME, skillfully predict its temporal variation.

Finally, we compare the circulation and SST anomalies associated with the EAJLI between the observation and

model predictions. The results show that the models can adequately capture the meridional shift of the Asian westerly jet in the upper troposphere and a meridional wave train over East Asia and the WNP in the lower troposphere, associated with the EAJLI. In addition, the warm SST anomalies in the tropical eastern Pacific and NIO related to the southward shift of the EAJ are also successfully captured, though their teleconnections are stronger in the model predictions than in the observation. Based on a statistical multiple linear regression model built on two model-predicted SST indices, representing the interannual variation of SST in the tropical eastern Pacific and NIO, respectively, we reproduce about half of the year-to-year variance of the model-predicted EAJLI, suggesting that the prediction skill of the EAJLI is contributed to significantly by the linear impact of the model-predicted tropical SST anomalies in the above two regions. The possible mechanisms linking the tropical SST anomalies to the interannual variation of the EAJ location are also discussed.

Acknowledgements. We thank two anonymous reviewers for their valuable comments. We also thank Dr. LU Riyu from the Institute of Atmospheric Physics, Chinese Academy of Sciences, for discussion during preparation of the manuscript. This research was supported by the National Natural Science Foundation of China (Grant Nos. 41375086, 41320104007 and 41305067).

REFERENCES

Adler, R. F., and Coauthors, 2003: The version-2 global precipitation climatology project (GPCP) monthly precipitation analysis (1979–Present). *Journal of Hydrometeorology*, **4**, 1147–1167.

Chowdary, J. S., S. P. Xie, J.-Y. Lee, Y. Kosaka, and B. Wang, 2010: Predictability of summer Northwest Pacific climate in 11 coupled model hindcasts: Local and remote forcing. *J. Geophys. Res.*, **115**, D22121, doi: 10.1029/2010JD014595.

Ding, Q. H., and B. Wang, 2005: Circumglobal teleconnection in the Northern Hemisphere summer. *J. Climate*, **18**, 3483–3505, doi: 10.1175/JCLI3473.1.

Doblas-Reyes, F. J., A. Weisheimer, T. N. Palmer, J. M. Murphy, and D. Smith, 2010: Forecast quality assessment of the ENSEMBLES seasonal-to-decadal Stream 2 hindcasts. *ECMWF Technical Memorandum*, No. 621, ECMWF, Reading, UK, 45 pp.

Dole, R. M., and R. X. Black, 1990: Life cycles of persistent anomalies. Part II: The development of persistent negative height anomalies over the North Pacific Ocean. *Mon. Wea. Rev.*, **118**, 824–846.

Enomoto, T., 2004: Interannual variability of the Bonin high associated with the propagation of Rossby waves along the Asian jet. *J. Meteor. Soc. Japan*, **82**, 1019–1034.

Enomoto, T., B. J. Hoskins, and Y. Matsuda, 2003: The formation mechanism of the Bonin high in August. *Quart. J. Roy. Meteor. Soc.*, **129**, 157–178.

Huang, G., 2004: An index measuring the interannual variation of the East Asian summer monsoon—The EAP index. *Adv. Atmos. Sci.*, **21**, 41–52, doi: 10.1007/BF02915679.

Huang, P., and R. H. Huang, 2009: Southern-Northern Hemispheres symmetric and asymmetric effect of El Niño events on general circulation and analysis on its mechanism. *Chinese J. Atmos. Sci.*, **33**, 1–15, doi: 10.3878/j.issn.1006-9895.2009.01.01. (in Chinese).

Huang, R. H., and F. Y. Sun, 1992: Impacts of the tropical western Pacific on the East Asian summer monsoon. *J. Meteor. Soc. Japan*, **70**, 243–256.

Kalnay, E., and Coauthors, 1996: The NCEP/NCAR 40-Year reanalysis project. *Bull. Amer. Meteor. Soc.*, **77**, 437–471.

Kosaka, Y., and H. Nakamura, 2006: Structure and dynamics of the summertime Pacific-Japan teleconnection pattern. *Quart. J. Roy. Meteor. Soc.*, **132**, 2009–2030.

Kosaka, Y., J. S. Chowdary, S. P. Xie, Y.-M. Min, and J.-Y. Lee, 2012: Limitations of seasonal predictability for summer climate over East Asia and the Northwestern Pacific. *J. Climate*, **25**, 7574–7589, doi: 10.1175/JCLI-D-12-00009.1.

Kumar, A., and M. P. Hoerling, 2003: The nature and causes for the delayed atmospheric response to El Niño. *J. Climate*, **16**, 1391–1403.

Lau, K.-M., K.-M. Kim, and S. Yang, 2000: Dynamical and boundary forcing characteristics of regional components of the Asian summer monsoon. *J. Climate*, **13**, 2461–2482.

Lee, J.-Y., B. Wang, Q. Ding, K.-J. Ha, J.-B. Ahn, A. Kumar, B. Stern, and O. Alves, 2011: How predictable is the northern hemisphere summer upper-tropospheric circulation? *Climate Dyn.*, **37**, 1189–1203, doi: 10.1007/s00382-010-0909-9.

Li, C. F., R. Y. Lu, and B. W. Dong, 2012: Predictability of the western North Pacific summer climate demonstrated by the coupled models of ENSEMBLES. *Climate Dyn.*, **39**, 329–346, doi: 10.1007/s00382-011-1274-z.

Li, C. F., R. Y. Lu, and B. W. Dong, 2014: Predictability of the western North Pacific summer climate associated with different ENSO phases by ENSEMBLES multi-model seasonal forecasts. *Climate Dyn.*, **43**, 1829–1845, doi: 10.1007/s00382-013-2010-7.

Liang, X. Z., and W.-C. Wang, 1998: Associations between China monsoon rainfall and tropospheric jets. *Quart. J. Roy. Meteor. Soc.*, **124**, 2597–2623, doi: 10.1002/qj.49712455204.

Lim, H., and C. P. Chang, 1983: Dynamics of teleconnections and walker circulations forced by equatorial heating. *J. Atmos. Sci.*, **40**, 1897–1915.

Lim, H., and C. P. Chang, 1986: Generation of internal-and external-mode motions from internal heating: Effects of vertical shear and damping. *J. Atmos. Sci.*, **43**, 948–960.

Lin, Z. D., 2010: Relationship between meridional displacement of the monthly East Asian jet stream in the summer and sea surface temperature in the tropical central and eastern Pacific. *Atmos. Oceanic Sci. Lett.*, **3**, 40–44.

Lin, Z. D., 2013: Impacts of two types of northward jumps of the East Asian upper-tropospheric jet stream in midsummer on rainfall in eastern China. *Adv. Atmos. Sci.*, **30**, 1224–1234, doi: 10.1007/s00376-012-2105-9.

Lin, Z. D., and R. Y. Lu, 2005: Interannual meridional displacement of the East Asian upper-tropospheric jet stream in summer. *Adv. Atmos. Sci.*, **22**, 199–211, doi: 10.1007/BF02918509.

Lu, R. Y., 2004: Associations among the components of the East Asian summer monsoon system in the meridional direction. *J. Meteor. Soc. Japan*, **82**, 155–165.

Lu, R. Y., and Z. D. Lin, 2009: Role of subtropical precipitation anomalies in maintaining the summertime meridional teleconnection over the western North Pacific and East Asia. *J. Climate*, **22**, 2058–2072.

Lu, R. Y., J.-H. Oh, and B.-J. Klim, 2002: A teleconnection pattern in upper-level meridional wind over the North African and Eurasian continent in summer. *Tellus*, **54A**, 44–55.

Lu, R. Y., Y. Li, and B. W. Dong, 2006: External and internal summer atmospheric variability in the western North Pacific and East Asia. *J. Meteor. Soc. Japan*, **84**, 447–462.

Lu, R. Y., Z. D. Lin, and Y. C. Zhang, 2013: Variability of the East Asian upper-tropospheric jet in summer and its impacts on the East Asian monsoon. *Chinese J. Atmos. Sci.*, **37**, 331–340, doi: 10.3878/j.issn.1006-9895.2012.12310. (in Chinese).

Nitta, T., 1987: Convective activities in the tropical western Pacific and their impact on the Northern Hemisphere summer circulation. *J. Meteor. Soc. Japan*, **65**, 373–390.

Qu, X., and G. Huang, 2012: Impacts of tropical Indian Ocean SST on the meridional displacement of East Asian jet in boreal summer. *Inter. J. Climatol.*, **32**, 2073–2080, doi: 10.1002/joc.2378.

Shaman, J., and E. Tziperman, 2007: Summertime ENSO-North African-Asian jet teleconnection and implications for the Indian monsoons. *Geophys. Res. Lett.*, **34**, L11702, doi: 10.1029/2006GL029143.

Smith, T. M., and R. W. Reynolds, 2004: Improved extended reconstruction of SST (1854–1997). *J. Climate*, **17**, 2466–2477.

van der Linden, P., and J. F. B. Mitchell, 2009: ENSEMBLES: Climate change and its impact: summary of research and results from ENSEMBLES project. Met Office Hadley Centre, FitzRoy Road, Exeter EX1 3PB, UK, 160 pp.

Wang, B., 2008: Thrusts and prospects on understanding and predicting Asian monsoon climate. *Acta Meteorologica Sinica*, **22**, 383–403.

Wang, B., and X. S. Xie, 1996: Low-frequency equatorial waves in vertically sheared zonal flow. Part I: Stable waves. *J. Atmos. Sci.*, **53**, 449–467.

Wang, B., I.-S. Kang, and J.-Y. Lee, 2004: Ensemble simulations of Asian-Australian monsoon variability by 11 AGCMs. *J. Climate*, **17**, 803–818.

Wang, B., Q. H. Ding, X. H. Fu, I.-S. Kang, K. Jin, J. Shukla, and F. Doblas-Reyes, 2005: Fundamental challenge in simulation and prediction of summer monsoon rainfall. *Geophys. Res. Lett.*, **32**, L15711, doi: 10.1029/2005GL022734.

Wang, W. W., W. Zhou, X. Wang, S. K. Fong, and K. C. Leong, 2013: Summer high temperature extremes in Southeast China associated with the East Asian jet stream and circumglobal teleconnection. *J. Geophys. Res.*, **118**, 8306–8319, doi: 10.1002/jgrd.50633.

Weisheimer, A., F. J. Doblas-Reyes, T. N. Palmer, A. Alessandri, A. Arribas, M. Déqué, N. Keenlyside, M. MacVean, A. Navarra, and P. Rogel, 2009: ENSEMBLES: A new multi-model ensemble for seasonal-to-annual predictions—Skill and progress beyond DEMETER in forecasting tropical Pacific SSTs. *Geophys. Res. Lett.*, **36**, L21711, doi: 10.1029/2009GL040896.

Wu, W. J., J. H. He, H.-S. Chung, C.-H. CHo, and R. Y. Lu, 2006: The relationship between the East Asian up-tropospheric jet stream in summer and climatic characteristics of synoptic-scale disturbance. *Climatic and Environmental Research*, **11**, 525–534. (in Chinese).

Xiang, Y., and X. Q. Yang, 2012: The effect of transient eddy on interannual meridional displacement of summer East Asian subtropical jet. *Adv. Atmos. Sci.*, **29**, 484–492, doi: 10.1007/s00376-011-1113-5.

Xie, S. P., K. M. Hu, J. Hafner, H. Tokinaga, Y. Du, G. Huang, and T. Sampe, 2009: Indian Ocean capacitor effect on Indo-Western Pacific climate during the summer following El Niño. *J. Climate*, **22**, 730–747.

Yu, R. C., and T. J. Zhou, 2007: Seasonality and three-dimensional structure of interdecadal change in the East Asian monsoon. *J. Climate*, **20**, 5344–5355, doi: 10.1175/2007JCLI1559.1.

Yulaeva, E., and J. M. Wallace, 1994: The signature of ENSO in global temperature and precipitation fields derived from the microwave sounding unit. *J. Climate*, **7**, 1719–1736.

Zhang, Y. C., and L. L. Guo, 2005: The deviation of the East Asian subtropical westerly jet and the simulation of seasonal variation of the East China rain bands. *Chinese Science Bulletin*, **50**, 1394–1399. (in Chinese).

Zhang, Y. C., and D. Q. Huang, 2011: Has the East Asian westerly jet experienced a poleward displacement in recent decades? *Adv. Atmos. Sci.*, **28**, 1259–1265, doi: 10.1007/s00376-011-9185-9.